Structural and electric properties of two semifluorinated alkane monolayers compressed on top of a controlled hydrophobic monolayer substrate

Abdel-Illah El Abed*
Laboratoire de Neuro-Physique Cellulaire, Université René Descartes, 45 rue des Saints-Pères, 75006 Paris, France

Radoslav Ionov
College of Science, Postal Box 946, BG-1000, Bulgaria

Michel Goldmann
Institut des Nano-Sciences de Paris (INSP), UMR-CNRS 7588, Universités Paris 6 et Paris 7, 140 rue de Lourmel, 75015 Paris, France

(Received 5 July 2007; published 24 October 2007)

We investigate the dynamic behavior upon lateral compression of two mixed films made with one of the two semifluorinated alkanes $F(CF_2)_8(CH_2)_{18}H$ and $F(CF_2)_{10}(CH_2)_{10}H$ and the natural α-helix alamethicin peptide. Surface pressure, surface potential versus molecular area isotherms, and grazing-incidence x-ray diffraction were applied to characterize this system. We show that both mixed films demix vertically to form two asymmetric flat bilayers where the lower layer is made of alamethicin and the upper layer is made of semifluorinated molecules. The structure matching of the semifluorinated alkanes (where the hydrophilic group is missing) with a suitable organization of the underlying alamethicin monolayer allows for a continuous compression of the upper semifluorinated layers while the density of the lower alamethicin monolayer remains constant. Comparing data of the two studied mixed films enables us to evaluate the effect of chain length on the in-plane organization of the molecules and on the electric properties of the upper layers.

DOI: 10.1103/PhysRevE.76.041606 PACS number(s): 68.18.−g, 68.65.Ac

I. INTRODUCTION

Binary mixtures of fluorocarbons and hydrocarbons have been largely studied since 1950 [1]. They generally form highly nonideal mixtures either in three-dimensional (3D) or 2D systems (see for a review Refs. [2,3]). Their nonmiscibility is often attributed to a difference in chain conformation between fluoroalkanes and alkanes and to the subsequent difference in their chains' cross sections. In fact, while $-(CH_2)_n-$ blocks adopt the all-trans conformation with a chain cross section of about 0.18 nm^2, fluorinated $-(CF_2)_n-$ blocks form (15/7) helices, which confers a greater rigidity and greater chain cross section of about 0.28 nm^2 [4]. From this point of view, the semifluorinated *n*-alkanes (SFA) $F(CF_2)_n(CH_2)_mH$ represent a particular system where the nonmiscible fluorocarbon and hydrocarbon are forced to coexist. Depending on *n* and *m* values, they may exhibit either solid or liquid-crystalline lamellar phases for which the molecular orientation determination appeared to be hard to achieve [5–12].

Another interesting feature of SFA is their ability to exhibit surface activity at the liquid alkane-air interface [13–16]. However, since the free energy of transfer of one $-CH_2-$ group from an alkane solvent to a perfluorinated alkane solvent (1.1 kJ mol^{-1}) is only one-third the energy needed to transfer a $-CH_2-$ group from an alkane solvent to water [14], attempts to form and study SFA monolayers at the liquid alkane-air interface, in the same manner as for classical amphiphile Langmuir films [13], have not been successful to our knowledge.

Surprisingly, some of SFA compounds are able to form genuine Langmuir monolayers at the air-water interface, as initially reported by Gaines [13] and studied in more detail later by many others [17–24]. Hence, mixed Langmuir films made of SFA and a suitable amphiphilic material may allow for the study of SFA monolayers on hydrophobic surfaces. For example, Krafft *et al.* [25] showed the occurrence upon compression of an original vertical phase separation in a mixture of the F_8H_{16} semifluorinated alkane and a phospholipid (DPPE). The observed vertical phase separation occurs at the collapse surface pressure of the pure F_8H_{16} monolayer—i.e., ~13 mN/m. This indicates that the organization of F_8H_{16} molecules at the air-water interface instead of the more suitable DPPE-air interface should be more likely governed by the minimizing of air-water interface surface tension. Later, El Abed *et al.* [26] showed, by means of surface pressure (π) versus molecular area (A) isotherms and x-ray reflectivity measurements, the occurrence of a new vertical phase separation in an original mixed Langmuir film made of the F_8H_{18} semifluorinated alkane and a natural α-helix alamethicin peptide (alam). In this case, the vertical phase separation appeared to occur at all surface pressures.

In this paper, we apply π-A isotherms, surface potential (ΔV)-A isotherms, and grazing-incidence x-ray diffraction (GIXD) measurements to characterize both the in-plane structure and the molecular orientation of two mixed Langmuir films made of alamethicin and two semifluorinated alkanes with different fluorocarbon and hydrocarbon blocks: namely, $F_{10}H_{10}$ and F_8H_{18}. In the bulk state, the $F_{10}H_{10}$ compound displays a smectic-B liquid-crystalline phase between 38 °C and 61 °C as initially shown by Mahler *et al.* [6] and for which different structural models were suggested, first by

*abdel.elabed@univ-paris5.fr

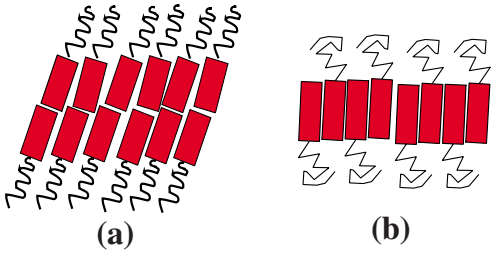

FIG. 1. (Color online) Schematic representation of structural models for the smectic-*B* phase of $F_{10}H_{10}$ suggested by (a) Viney *et al.* [9] and by (b) Tournilhac *et al.* [11].

Viney *et al.* [9] and later by Tournilhac *et al.* [11], as sketched in Figs. 1(a) and 1(b), respectively.

F_8H_{18} exhibits a crystalline phase which melts to an isotropic liquid at a temperature equal to 53 °C. The existence of a smectic phase was shown to be possible in the F_8H_m series only for $m \leq 12$ [12].

We show in this study that both F_8H_{18} and $F_{10}H_{10}$ molecules form stable monolayers at the top of the hydrophobic alamethicin monolayer, whereas at the air-water interface only F_8H_{18} molecules form also stable Langmuir monolayers. Moreover, the structure matching of the semifluorinated alkanes with a suitable organization of the underlying alamethicin monolayer allowed for a continuous compression of the upper F_8H_{18} monolayer while the density of the lower alamethicin monolayer remains constant. Thanks to x-ray diffraction data, we show that F_8H_{18} molecules organize in a quasirectangular 2D lattice whereas no long-range positional order could be detected in the $F_{10}H_{10}$ monolayer. Also, thanks to surface potential (ΔV) versus molecular area (A) measurements, we establish a direct correlation between the in-plane organization of the upper semifluorinated monolayer and its measured effective electric dipole moment.

II. EXPERIMENT

The F_8H_{18} and $F_{10}H_{10}$ compounds used were synthesized and purified (>98%) by Michèle Sanière from the Laboratoire de Chimie Pharmacologique et Toxicologique at Paris-Descartes University. Their preparation was carried out according to a well-known procedure [5].

The rodlike α-helix alamethicin is a natural antibiotic peptide constituted by 19 amino-acid residues and one amino alcohol. It may be approximated by a cylinder of 1.0 nm diameter and 3.0 nm height. The biological property of alamethicin relies on its amphiphilic feature and its ability to form ionic channels across the biological cell membrane. The peptide is amphiphilic since its polar hydrophilic groups are either at the C-terminus or lie along a narrow hydrophilic strip parallel to the helix axis. The used alamethicin compound was purchased from Sigma (Mw. 1959.9) and used as received.

Surface pressure (π) and surface potential (ΔV) versus molecular area A isotherms were recorded simultaneously using a Langmuir trough purchased from Nima Technology Ltd. The surface pressure was measured using a Wilhelmy plate with an accuracy of about 0.1 mN/m. The surface potential sensor consists of a commercial Kelvin probe with an area of 0.2 cm^2 which is suspended above the film spread at the air-water interface. Surface potential and molecular areas were measured with an accuracy of 30 mV and 5%, respectively. Monolayers were spread from chloroform solutions on a pure water surface (pH=5.7) and compressed at T =20 °C.

One could plot surface pressure π of mixed films versus the mean molecular area A of the two used amphiphile molecules. In our study, since the two mixed molecules organize each in two different planes as shown hereafter, it is more significant to plot surface pressure π versus individual molecular areas: namely, A_F or A_{alam}. These are determined simply by dividing the overall film area by the number of either F_nH_m molecules (n_F) or alamethicin molecules (n_{alam}), respectively. For instance, to convert the molecular area axis of the isotherm diagram from A_F to A_{alam}, one should multiply A_F values by the molecular mixture ratio $R_{F_nH_m/alam}=\frac{n_F}{n_{alam}}$.

Grazing-incidence x-ray diffraction was performed on the D41B beamline at the LURE synchrotron source (Orsay, France). The experimental setup is completely described in Ref. [27]. The x-ray wavelength $\lambda=1.646$ Å of the incoming x-ray beam was selected using a focusing Ge(111) monochromator. The intensity of the x-ray beam scattered by the monolayer was monitored vertically using a vertical gas-filled ($Ar-CO_2$) linear position-sensitive detector (PSD) (13°) as a function of the in-plane component of the scattering wave vector Q_{xy} selected by means of a Soller slit collimator. The study of the Q_{xy} pattern integrated over the vertical wave vector component Q_z allowed us to determine the 2D lattice of the alamethicin helices and the fluorinated chains, while the shape of the Bragg rods gave information about the tilt and azimuthal angles. The resolution in the wave vector transfer, Q_{xy}, is about 0.01 $Å^{-1}$ [full width at half maximum (FWHM)]. The integration range along Q_z is from 0 to 0.8 $Å^{-1}$ owing to the vertical size of Soller slits.

III. RESULTS

A. Surface pressure π versus molecular area A isotherm diagrams

We would like first to briefly recall the structural properties of the pure alamethicin Langmuir monolayer previously discussed in detail [28,29]. Curve (a) of Fig. 2 shows the π-A isotherm of the pure alamethicin monolayer. The peptide molecules spread spontaneously at the air-water interface and lead upon compression to the formation of a 2D solid phase at a molecular area of about 3.20 nm^2 corresponding to a surface pressure of about 20 mN/m. In this phase, molecules organize with their α-helix axis parallel to the air-water interface. On further compression to apparent molecular areas smaller than 3.20 nm^2, the π-A isotherm exhibits a plateau region where alamethicin molecules start to solubilize progressively into the water subphase. This is an important feature in our system as the molecular density of the alamethicin monolayer remains constant in this region.

Figures 2 and 3 show the surface pressure π-A isotherms of both mixed alam/$F_{10}H_{10}$ and alam/F_8H_{18} films, plotted, at

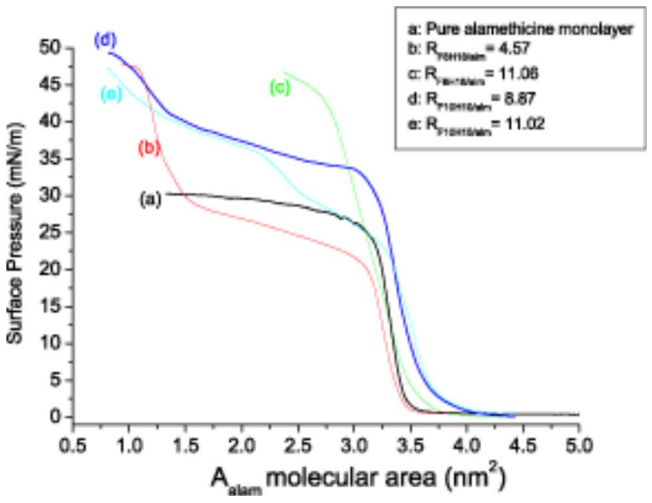

FIG. 2. (Color online) Surface pressure π versus A_{alam} molecular area isotherm diagrams, obtained on compressing mixed films of F_8H_{18}/alamethicin and $F_{10}H_{10}$/alamethicin made at different molecular mixture ratios $R_{\text{F/alam}}$; the compression speed was about 0.04 nm^2/min/molecule and the temperature was set at $T=20\,^{\circ}\text{C}$. Curve (a): pure alamethicin monolayer. Curve (b): $R_{\text{F/alam}}=2.46$. Curve (c): $R_{\text{F/alam}}=3.68$. Curve (d): $R_{\text{F/alam}}=7.06$. Curve (e): $R_{\text{F/alam}}=11.06$. Curve (f): pure F_8H_{18} monolayer. To convert the x axis from A_{F} values to A_{alam} values, one should multiply A_{F} values by $R_{\text{F/alam}}$.

different $R_{F_nH_m/\text{alam}}$ values, versus A_{alam} and A_{F}, respectively. Figure 2 shows clearly that, for both alam/F_8H_{18} and alam/$F_{10}H_{10}$ films, the first increase in surface pressure occurs practically at an alamethicin molecular area value of about $A_{\text{alam}}\sim 3.5\ \text{nm}^2$, similar to the molecular area of a pure

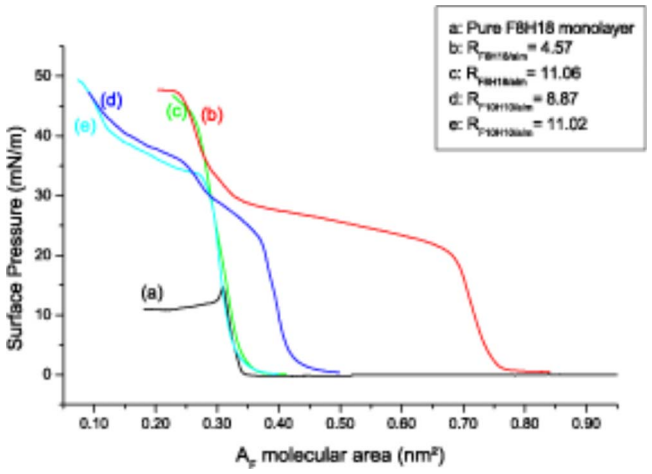

FIG. 3. (Color online) Surface pressure π versus A_{F} molecular area isotherm diagrams, obtained on compressing mixed films of F_8H_{18}/alamethicin and $F_{10}H_{10}$/alamethicin made at different molecular mixture ratios $R_{\text{F/alam}}$; the compression speed was about 0.04 nm^2/min/molecule and the temperature was set at $T=20\,^{\circ}\text{C}$. Curve (a): pure F_8H_{18} monolayer. Curve (b): $R_{\text{F/alam}}=2.46$. Curve (c): $R_{\text{F/alam}}=3.68$. Curve (d): $R_{\text{F/alam}}=7.06$. Curve (e): $R_{\text{F/alam}}=11.06$. To convert the x axis from A_{F} values to A_{alam} values, one should multiply A_{F} values by $R_{\text{F/alam}}$.

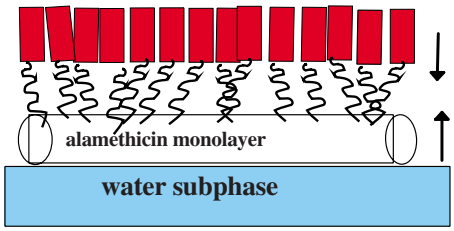

FIG. 4. (Color online) Schematic representation of the suggested model for the organization of the upper semifluorinated alkane monolayers built on the top of the hydrophobic surface of the underlying alamethicin monolayer. Arrows indicate the direction of the molecular dipole moments.

alamethicin monolayer. Moreover, if one plots π versus A_{F}, as shown in Fig. 3, one notices that the second increase in surface pressure occurs practically at a molecular area value of about $A_{\text{F}}\sim 0.3\ \text{nm}^2$, very close to the molecular area A_{F_0} of a pure F_8H_{18} monolayer in its condensed phase [see curve (a) of Fig. 3]. We underline that $F_{10}H_{10}$ molecules do not form stable monolayers at the air-water interface.

These results indicate that both $F_{10}H_{10}$/alamethicin films and F_8H_{18}/alamethicin films form asymmetric bilayers. Considering the hydrophilic character of alamethicin, it seems reasonable to consider it as forming the first layer, covering the water surface and covered by the second layer made of F_8H_{18} and $F_{10}H_{10}$ molecules (as represented in Fig. 4): the first increase of surface pressure π corresponds to the onset of a dense monolayer of alamethicin and the second increase of π corresponds to the onset of a dense monolayer of F_8H_{18} or $F_{10}H_{10}$.

Taking into account alamethicin and F_nH_m molecular sections, a particular mixture ratio should be obtained with $R_{F_nH_m/\text{alam}}\sim 11$: at this value, one should expect a simultaneous onset of dense layers for both alamethicin and F_nH_m molecules. The experimental π-A isotherm diagrams recorded at this molecular ratio are in good agreement with this statement; see curves (c) and (e) of Figs. 2 and 3.

On further compression, the alam/F_8H_{18} film shows a rapid and regular increase of π to a value of about 45 mN/m (at $A_{\text{F}}\sim 0.28\ \text{nm}^2$) followed by a collapse of the film. For this phase, the compressibility $\chi=-\frac{1}{A}\left(\frac{dA}{d\pi}\right)$ is measured at about 13 m N^{-1}, typical of condensedlike monolayers. In the case of the $F_{10}H_{10}$/alamethicin film, a further compression leads to a second break in π variation which indicates the occurrence of a phase transition. Then, the surface pressure increases rapidly at a molecular area of about $A_{\text{F}}\sim 0.14\ \text{nm}^2$ and a surface pressure of about $\pi=40$ mN/m. The molecular area value at which such a phase transition occurs indicates the formation of a second layer of $F_{10}H_{10}$ molecules as we will confirm in the present study using surface potential measurements.

B. Surface pressure ΔV versus molecular area A isotherm diagrams

Classical Langmuir monolayers can be assimilated generally to arrays of electric dipoles whose density and orienta-

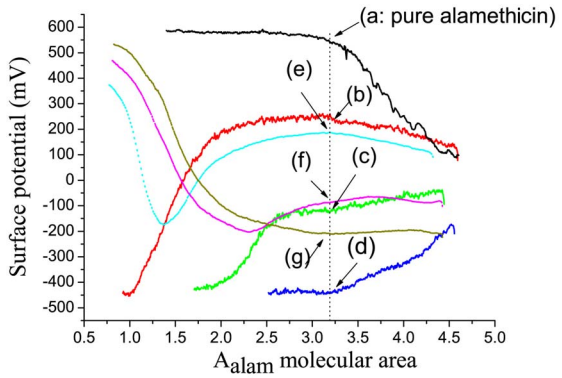

FIG. 5. (Color online) Surface potential ΔV versus molecular area A_{alam} isotherm diagrams of the pure alamethicin monolayer [curve (a)], of the F_8H_{18}/alamethicin mixed film [curve (b): $R_{F_8H_{18/alam}}=3.68$, curve (c): $R_{F_8H_{18/alam}}=7.06$, curve (d): $R_{F_8H_{18/alam}}=11.06$] and of the $F_{10}H_{10}$/alamethicin mixed film [curve (e): $R_{F_{10}H_{10/alam}}=5.548$, curve (f): $R_{F_{10}H_{10/alam}}=8.87$, curve (g): $R_{F_{10}H_{10/alam}}=11.06$]. The vertical dot line shows the A_{alam} molecular area value, 3.20 nm^2, at which ΔV values were measured for different mixed films used to plot ΔV versus A_F^{-1} as represented in Fig. 6.

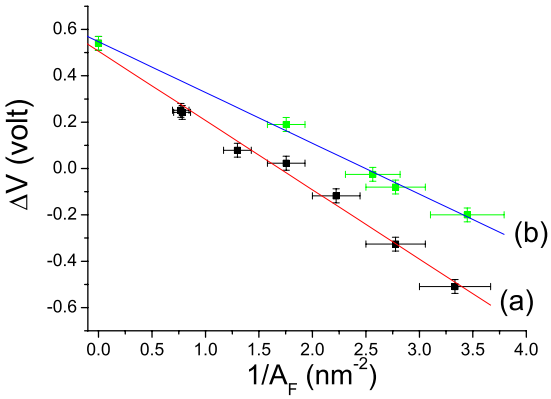

FIG. 6. (Color online) Plots of surface potential ΔV vs A_F^{-1} measured at a fixed alamethicin molecular area, $A_{\text{alam}}=3.20$ nm^2, for mixed F_8H_{18}/alamethicin films [curve (a)] and mixed $F_{10}H_{10}$/alamethicin films [curve (b)] for which $R_{F_nH_m/alam}$ varies from 2.5 to 11 approximately.

tion may change upon compression (see for a review Ref. [30]). The surface potential ΔV of a nonionized monolayer may be calculated, at a given molecular area A, according to the Helmholtz formula $\Delta V=\frac{\mu_\perp}{\varepsilon_0 \epsilon A}$, where $\mu_\perp$ is the average vertical component of the molecular dipole moment μ, ϵ_0 is the permittivity of the free space, and ϵ is the relative dielectric constant of the monolayer. Basically, the monolayer electric parameter which can be readily deduced from surface potential measurements is the *effective* molecular dipole $\frac{\mu_\perp}{\epsilon}$.

ΔV-A isotherm diagrams of the pure alamethicin Langmuir monolayer and also of the two alam/F_8H_{18} and alam/$F_{10}H_{10}$ mixed films measured for different $R_{F/alam}$ ratios are presented in Fig. 5. A surface potential value of $\Delta V=0.540$ mV is measured at $A_{\text{alam}}=3.20$ nm^2 for the pure alamethicin monolayer [curve (a)]. As we stated above, alamethicin molecules lay with their long helix axis parallel to the air-water interface; hence, the measured surface potential ΔV is proportional to the normal component $\mu_{\text{alam},\perp}$ of the alam electric-dipole moment by regards to the long axis of its helix. The positive sign of the recorded ΔV shows that $\mu_{\text{alam},\perp}$ is oriented upward—i.e., from the water subphase towards the air. Applying the Helmholtz formula for $\Delta V=540$ mV and $A_{\text{alam}}=3.20$ nm^2, one obtains $\frac{\mu_{\text{alam},\perp}}{\epsilon}=4.62$ D, which is much smaller than the parallel component of the alamethicin electric dipole moment [31]: $\mu_{\text{alam},\parallel}=75$ D.

On compressing further the alamethicin monolayer in the collapse region, the surface potential remains constant. This result confirms that the alamethicin monolayer density remains constant during the collapse process.

Curves (b)–(d) of Fig. 5 correspond to the ΔV-A isotherm diagrams of the alam/F_8H_{18} film recorded, respectively, for $R_{F_8H_{18/alam}}=3.68$, 7.06, and 11.06. Curves (e)–(g) correspond to the ΔV-A isotherm diagrams of the alam/$F_{10}H_{10}$ film recorded, respectively, for $R_{F_{10}H_{10/alam}}=5.54$, 8.87, and 11.09. As we can notice, the greater the density of the upper F_8H_{18} and $F_{10}H_{10}$ monolayers, the lower the surface potential of the mixed film. Since surface potential of the pure alamethicin monolayer is positive, such a result indicates that the surface potential of the upper F_8H_{18} and $F_{10}H_{10}$ layers are negative and thus both F_8H_{18} and $F_{10}H_{10}$ molecules should orient their electric dipole moment downward; i.e., fluorinated segments should be oriented upward and hydrocarbon segments should be oriented downward (see Fig. 4).

Following the Demchak-Fort electric model [32] for Langmuir monolayers, one may consider the F_nH_m/alamethicin bilayer as two layers of two different electric-dipole moments and two different dielectric constants: $\mu_1=\mu_{\text{alam}}$, $\epsilon_1=\epsilon_{\text{alam}}$, and $\mu_2=\mu_F$, $\epsilon_2=\epsilon_F$ for the alamethicin and the F_nH_m layers, respectively. Thus,

$$\varepsilon_0 \Delta V = \frac{\mu_1}{\varepsilon_1 A_1} + \frac{\mu_2}{\varepsilon_2 A_2}.$$

Since $\frac{\mu_1}{\varepsilon_1}=\frac{\mu_{\text{alam},\perp}}{\varepsilon_{\text{alam}}}=4.62$ D, the above equation becomes at $A_1=A_{\text{alam}}=3.20$ nm^2:

$$\Delta V = 0.54 + \frac{1}{2.65}\left(\frac{\mu_2}{\varepsilon_2}\right)\frac{1}{A_2},$$

where ΔV, μ_2, and A_2 are expressed in volts, debyes, and nm^2, respectively.

Experimentally, a plot of ΔV vs A_F^{-1} measured at a fixed $A_{\text{alam}}=3.20$ nm^2 shows clearly a linear decrease of ΔV vs the density of either the F_8H_{18} layer [Fig. 6(a)] or the $F_{10}H_{10}$ layer [Fig. 6(b)]. This linear variation is a direct proof of the validity of our model.

Moreover, the determination of the experimental slope of the linear curve ΔV vs A_F^{-1} allows for a direct estimation of the vertical component of the mean effective electric dipole of $F_{10}H_{10}$ and F_8H_{18} molecules in the upper layers:

$$\frac{(\mu_{F_{10}})_z}{\varepsilon_{F_{10}}} = -0.60 \text{ D}, \quad \frac{(\mu_{F_8})_z}{\varepsilon_{F_8}} = -0.76 \text{ D}.$$

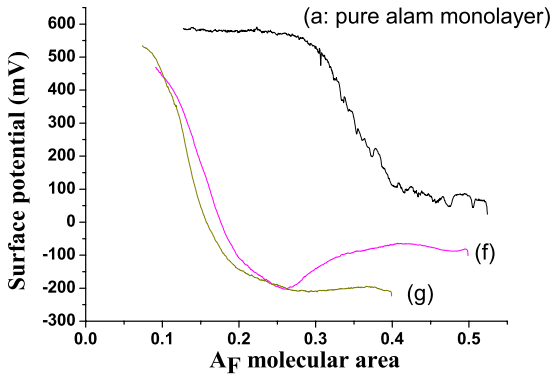

FIG. 7. (Color online) Plots of surface potential ΔV vs A_F for two mixed $F_{10}H_{10}$/alamethicin films: curve (f): $R_{F_{10}H_{10/alam}}=8.87$. Curve (g): $R_{F_{10}H_{10/alam}}=11.06$. Curve (a): pure alamethicin monolayer for which the x axis is arbitrary.

We remark that the vertical component of the mean molecular effective electric dipole is significantly greater for the F_8H_{18} monolayer than for the $F_{10}H_{10}$ monolayer. Assuming that both $F_{10}H_{10}$ and F_8H_{18} layers possess the same relative dielectric constant, which may be taken equal to $\varepsilon_F \simeq 4.5$ as reported previously for F_8H_{18} [26] and for F_6H_6 [33], the observed difference between the two measured values of the vertical component of the mean molecular effective electric dipoles should be attributed to a difference in the orientation of molecules of F_8H_{18} and $F_{10}H_{10}$ molecules by regards to the normal to the layers surfaces. This particular point is discussed in more detail in the next section thanks to grazing's incidence x-ray data.

Another interesting result obtained from the analysis of surface potential measurements of alam/$F_{10}H_{10}$ films is the inversion and the rapid increase of surface potential at small molecular area values. Plotting ΔV versus A_F gives a better view of such variation as represented in Fig. 7. We attribute such result to the building of a second layer of $F_{10}H_{10}$ molecules on the top of the first one. In such a manner that the electric-dipole moments of the first and the second layers of $F_{10}H_{10}$ molecules are antiparallel as represented in Fig. 8. Our suggested structural model for the built-in $F_{10}H_{10}$ bilayer is compatible with the structural model suggested by Viney

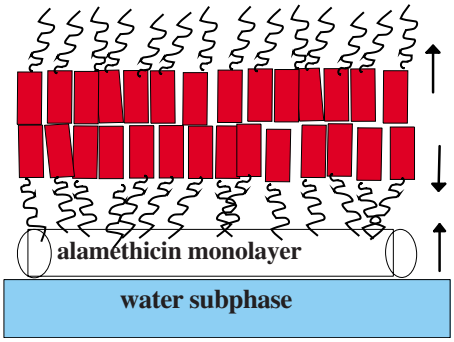

FIG. 8. (Color online) Schematic representation of the suggested model for the organization of the $F_{10}H_{10}$ bilayer built at small molecular areas on the top of the alamethicin monolayer. Arrows indicate the direction of the molecular dipole moments.

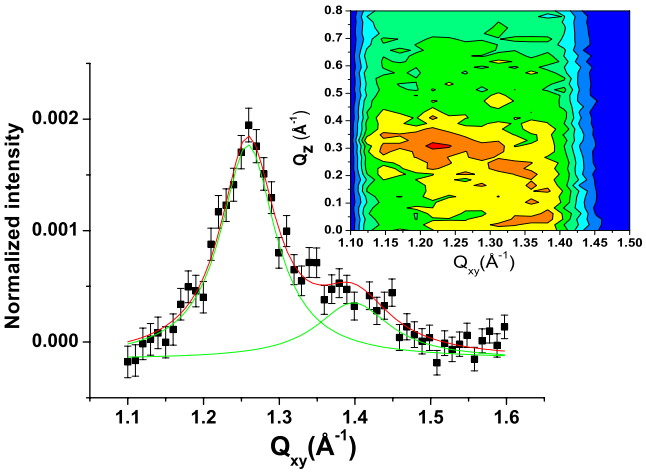

FIG. 9. (Color online) X-ray diffraction pattern of the F_8H_{18} layer recorded at $\pi=30$ mN/m: two diffraction peaks at 1.257 and 1.384 Å^{-1} are observed. Inset shows the contour plot diagram. The lattice which contains two chains is rectangular with $a=0.599$ nm, $b=0.908$ nm, and $\gamma=90°$.

et al. [9] for the smectic-*B* phase displayed in the bulk state by the $F_{10}H_{10}$ compound.

C. Grazing-incidence x-ray diffraction

In order to characterize the in-plane organization of the F_8H_{18} and $F_{10}H_{10}$ layers at the air-alamethicin interface, we performed synchrotron GIXD experiments on mixed films at different surface pressure values. In this paper, we discuss results of 2θ scans recorded around 1.26 Å^{-1} where one expects to observe diffraction peaks of close-packed fluorinated chains.

Figure 9 shows a typical scan performed on the F_8H_{18} layer at $A_F=0.32$ nm^2. One detects two large diffraction peaks at the following in-plane scattering wave vectors Q_{xy}: 1.257 Å^{-1} and 1.384 Å^{-1}. The observation of two diffraction peaks can be indexed as two peaks of a rectangular lattice which contains two molecules per unit cell and defined by $a=0.599$ nm, $b=0.908$ nm, and $\gamma=90°$. From the lattice parameters, one deduces an area per unit cell A_c equal to 0.54 nm^2 and an area per molecule of 0.27 nm^2. As we can notice, this value is very close to the cross section of fluorinated chains. The diffracting planes correspond to the organization of the fluorinated chains. The full widths at half maximum of the above diffraction peaks are 0.080 and 0.094 Å^{-1}, from which one could deduce a weak correlation length value $L=\frac{2\pi}{\text{FWHM}} \sim 80$ Å.

Rod scans show a maximum intensity for the in-plane scattering wave vectors at approximately $Q_z=0.3$ Å^{-1} for $Q_{xy}=1.257$ Å^{-1} and zero for $Q_{xy}=1.384$ Å^{-1}, which indicate that the fluorinated chains are oriented more or less normal to the air-water interface—i.e., 15° in regard to the normal to the air-water interface.

We also note that the FWHM (ΔQ_z) of the rod scans, taken in the cut through the peak at $Q_{xy}=1.257$ Å^{-1}, leads to a thickness of the diffracting fluorocarbon slab of about h

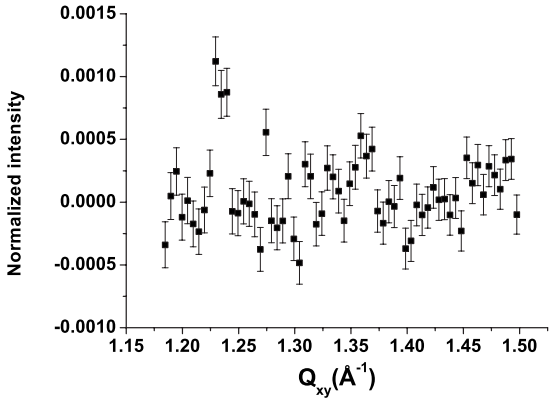

FIG. 10. X-ray diffraction pattern of the $F_{10}H_{10}$ layer recorded at $\pi=32$ mN/m where one could distinguish two peaks at around 1.23 and 1.37 $Å^{-1}$.

$=\frac{2\pi}{\Delta Q_z}\simeq 0.98$ nm, close to the calculated length of the fluorinated chain: 1.2 nm.

We underline that such rectangular lattices for F_8H_{18} molecules organize is unexpected since they form rather distorted hexagonal packing at the air-water interface [34]. Nevertheless, such rectangular lattices should be induced by the 2D crystalline underlying alamethicin monolayer which forms also a rectangular lattice [28,29]. Induced crystalline order in a nonordered phospholipid Langmuir monolayer by adsorbed charged nanocrystals made of the disk-shaped inorganic compound Laponite has been reported recently [35].

In the case of the $F_{10}H_{10}$/alamethicin film, the diffraction pattern represented in Fig. 10 exhibits a large noise/signal ratio which makes it difficult to fit and to discuss in detail the recorded GIXD spectrum. Nevertheless, one may probably distinguish again the presence of two peaks at around 1.23 and 1.37 $Å^{-1}$. We think that the almost absence of diffraction peaks in this case should be attributed to the fact that, unlike the F_8H_{18} monolayer layer, the $F_{10}H_{10}$ monolayer is in a liquidlike state.

IV. CONCLUSION

We showed in this paper that both mixed alam/F_8H_{18} and alam/$F_{10}H_{10}$ films exhibit a spontaneous vertical phase separation upon compression. They form two asymmetric flat bilayers where the lower layer is made of alamethicin and the upper layer is made of semifluorinated molecules. We showed also that the suitable collapse properties of the underlying alamethicin monolayer allow for a continuous compression of the F_8H_{18} and $F_{10}H_{10}$ monolayers on the top of the alamethicin monolayer. Analyzing the data of surface pressure versus molecular area and grazing-incidence x-ray diffraction measurements enabled us to compare the properties of the two semifluorinated monolayers: whereas F_8H_{18} molecules form a quasi-2D rectangular crystalline monolayer, $F_{10}H_{10}$ molecules may form a liquidlike monolayer. Also, we established a direct correlation between the in-plane organization and the measured effective electric-dipole moments of the semifluorinated monolayers.

Finally, our results indicate that the olephobic-olephilic balance plays an important role in the ability of semifluorinated molecules to form monolayers on hydrophobic surfaces and also to control the molecular orientation. Molecules with small fluorocarbon and long hydrocarbon blocks (F_8H_{18}) adopt at all surface pressures a parallel organization with hydrocarbon blocks in contact with the hydrophobic substrate, whereas molecules with long fluorocarbon and small hydrocarbon blocks ($F_{10}H_{10}$) adopt a parallel orientation at lower surface pressures and form an antiparallel second layer of molecules at higher surface pressures.

[1] J. H. Hilderbrand, B. B. Fisher, and H. A. Benesi, J. Am. Chem. Soc. **72**, 4348 (1950).
[2] J. P. Mukerjee and A. Y. S. Yang, J. Phys. Chem. **80**, 1388 (1976).
[3] P. Lo Nostro, Adv. Colloid Interface Sci. **56**, 245 (1995).
[4] C. W. Bunn and E. R. Howell, Nature (London) **174**, 549 (1954).
[5] J. F. Rabolt, T. P. Russell, and R. Twieg, Macromolecules **17**, 2786 (1984).
[6] W. Mahler, D. Guillon, and A. Skoulios, Mol. Cryst. Liq. Cryst., Lett. Sect. **2**, 111 (1985).
[7] J. Höpken and M. Möller, Macromolecules **25**, 2482 (1992).
[8] T. P. Russel, J. F. Rabolt, R. J. Twieg, and R. L. Siemens, Macromolecules **19**, 1135 (1986).
[9] C. Viney, T. P. Russell, L. E. Depero, and R. J. Twieg, Mol. Cryst. Liq. Cryst. **168**, 63 (1989).
[10] P. Marczuck and P. Lang, Macromolecules **31**, 9013 (1998).
[11] F-G. Tournilhac, P. Bassoul, and R. Cortes, Mol. Cryst. Liq. Cryst. Sci. Technol., Sect. A **362**, 45 (2001).
[12] M. Broniatowski, P. Dynarowicz-Latka, and W. Witko, Mol. Cryst. Liq. Cryst. **460**, 63 (2006).
[13] G. Gaines, Jr., *Insolubles Monolayers at Liquid-Gas Interfaces* (Interscience, New York, 1966).
[14] B. P. Binks, P. D. I. Fletcher, S. N. Kotsev, and R. L. Thompson, Langmuir **13**, 6669 (1997).
[15] P. Marczuk, P. Lang, and M. Möller, Colloids Surf., A **163**, 103 (2000).
[16] Y. Hayami and H. Sakamoto, Colloid Polym. Sci. **282**, 461 (2004).
[17] G. L. Gaines, Jr., Langmuir **7**, 3054 (1991).
[18] Z. Huang, A. A. Acero, N. Lei, S. Rice, Z. Zhang, and M. Schlosmann, J. Chem. Soc., Faraday Trans. **92**, 545 (1996).
[19] A. El Abed, E. Pouzet, M-C. Fauré, M. Sanière, and O. Abillon, Phys. Rev. E **62**, R5895 (2000).
[20] A. El Abed, M-C. Fauré, E. Pouzet, and O. Abillon, Phys. Rev. E **65**, 051603 (2002).
[21] M. Maaloum, P. Muller, and M-P. Krafft, Angew. Chem., Int. Ed. **41**, 4331 (2002).
[22] P. Lo Nostro, Curr. Opin. Colloid Interface Sci. **8**, 223 (2003).
[23] P. Fontaine, M. Goldmann, P. Muller, M-C. Fauré, O. Konov-

alov, and M-P. Krafft, J. Am. Chem. Soc. **127**, 512 (2005).
[24] M. Broniatowski, I. Sandez Macho, and P. Dynarowicz-Latka, Thin Solid Films **493**, 249 (2005).
[25] M. P. Krafft, F. Giulieri, P. Fontaine, and M. Goldmann, Langmuir **17**, 6577 (2001).
[26] A. I. El Abed, R. Ionov, M. Daoud, and O. Abillon, Phys. Rev. E **70**, 051607 (2004).
[27] P. Fontaine, M. Goldmann, M. Bordessoule, and A. Jucha, Rev. Sci. Instrum. **75**, 3097 (2004).
[28] R. Ionov, A. El Abed, A. Angelova, M. Goldmann, and P. Peretti, Biophys. J. **78**, 3026 (2000).
[29] R. Ionov, A. El-Abed, M. Goldmann, and P. Peretti, J. Phys. Chem. B **108**, 8485 (2004).
[30] D. M. Taylor, Adv. Colloid Interface Sci. **87**, 183 (2000).
[31] S. Stankowski, U. D. Schwarz, and G. Schwarz, Biochim. Biophys. Acta **11**, 941 (1988).
[32] R. J. Demchak and T. J. Fort, Jr., J. Colloid Interface Sci. **46**, 191 (1974).
[33] A. Hariharan and J. G. Harris, J. Chem. Phys. **101**, 4156 (1994).
[34] A. El Abed, M-C. Fauré, P. Fontaine, and M. Goldmann (unpublished).
[35] L. Wiegart, S. M. O'Flaherty, and B. Struth, Langmuir **21**, 1695 (2005).